# An Interference Rejection Filter For An Ultra-Wideband Quadrature Downconversion Autocorrelation Receiver

Sumit Bagga, Sandro A. P. Haddad, Koen van Hartingsveldt, Simon Lee, Wouter A. Serdijn and John R. Long
Electronics Research Laboratory, Faculty of Electrical Engineering, Mathematics and Computer Science,
Delft University of Technology,
Delft, The Netherlands
E-mail: {s.bagga, s.haddad, k.vanhartingsveldt, w.a.serdijn, j.r.long}@ewi.tudelft.nl

***Abstract*—An analog filter is designed based upon the requirement of an interference rejection filter for the Quadrature Downconversion Autocorrelation Receiver (QDAR). The transfer function of an eight-order elliptic band-pass filter is selected. As a result, a state-space approach (i.e. the orthonormal form [1]) is adopted, which is intrinsically semi-optimized for dynamic range, has low sensitivity, high sparsity and its coefficients can be physically implemented. Each coefficient in the state-space description of the filter is implemented at circuit level using a novel 2-stage gm cell based upon the principle of negative feedback. Simulation results in IBM's Bi-CMOS 0.18 μm technology show that the interference rejection filter requires a total current of 90 mA at a 1.8 V power supply. The 1-dB compression point of the filter is at 565 mV and the SNR is 47.5 dB. On performing a Monte Carlo simulation, it becomes evident that the overall filters transfer response does not suffer from process variations.**

*Keywords*—ultra-wideband, narrowband interference, state-space synthesis, orthonormal filter, quadrature downconversion autocorrelation receiver, analog integrated circuits

## I. INTRODUCTION

Although impulse radio ultra-wideband technology promises enhanced data throughput with low-power consumption, it inseparably introduces several challenging design issues. Ultra-wideband systems transmit at very low spectral densities and occupy a large amount of bandwidth, thus it is unequivocal that interference introduced from neighboring narrowband systems is a serious predicament, which could severely hamper or even degrade the overall performance of the system.

Among currently investigated UWB receiver architectures, the transmitted reference scheme proposed by Hoctor and Tomlinson [2] resolves the issue not only of synchronization but also of multipath components. In this scheme, consecutive pulses are transmitted with a predefined delay τ between them. The first pulse acts as a reference, whereas the second pulse is modulated. The autocorrelation receiver correlates the incoming signal with a delayed version of itself. The absolute value of the output after integration is in fact the energy of the pulse while the polarity of the output contains the data. The issue of narrowband interference led us to the design of novel receiver architecture i.e. the quadrature downconversion autocorrelation receiver (QDAR) (see Fig. 1.) [3], which is capable of operating in the presence of strong narrowband interference. It uses the property of frequency wrapping or in other words, it folds the ultra-wideband frequency spectrum around the origin. At the same time, interferers are positioned outside the band of interest and can be simply removed by the means of a band-pass filter (see Figure 2). Even though the bandwidth reduces significantly and the shape of the transmitter pulse is distorted, the QDAR makes use of the fact that detection with an autocorrelation receiver is feasible as long as the relative polarity and shape of consecutive pulses is preserved.

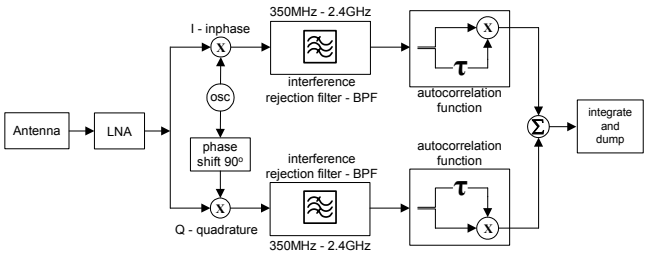


Fig. 1. Quadrature downconversion autocorrelation receiver (QDAR)

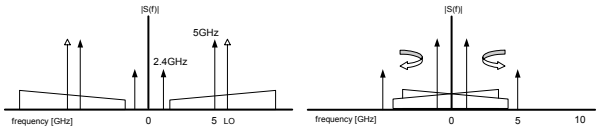


Fig. 2. left) frequency spectrum before downconversion and right) after downconversion

This paper proposes an interference rejection (i.e. an eighth order elliptic band pass) filter to be used in the QDAR (see Fig. 1). Section 2 relates the transformation procedure of the transfer function of the band pass filter into the orthonormal state-space form. Transconductance amplifiers are frequently employed in filters designed for high-frequency applications, and are employed in this particular case of impulse radio ultra-wideband circuit design. Section 3 describes the design and implementation of the 2-stage negative feedback transconductance cell. Simulation data of the transconductance amplifier as well as the overall filter transfer is given in Section 4. Section 5 presents the conclusions.

## II. FILTER DESIGN

### A. Transfer function and state-space synthesis

The analysis in [3] showed that, after downconversion, the interferer moves adjacent to the band of interest. The 5 GHz interferer appears below 350 MHz and the 2.4 GHz interferer beyond 3.1 GHz, when down-converting with an oscillator frequency of 5.5 GHz.

Trade-offs between slope, attenuation and circuit complexity are taken into consideration prior to choosing the order of the filter. An elliptic filter gives the steepest slope for any given order and is therefore the appropriate choice. The abovementioned extenuates the requirement for an eighth order elliptic band-pass filter. The transfer function (see below) of the interference rejection filter is generated using Matlab. The corner frequencies are set at 350 MHz and 2.6 GHz. The stop-band attenuation is at least 20 dB and the pass-band ripple is 0.5 dB.

$$H(s)=\left[\frac{0.1s^8-5.93e-7s^7+1.43e20s^6-1.03e15s^5+3.82e40s^4-3.71e34s^3+1.87e59s^2-2.8e52s+1.71e77}{s^8+1.62e10s^7+5.23e20s^6+5.04e30s^5+6.53e40s^4+1.82e50s^3+6.88e59s^2+7.64e68s+1.71e78}\right]$$

Once the desired transfer function is formulated, its state-space description is then determined. A state-space description for a given transfer function is not unique, meaning that many state-space descriptions can implement the same transfer function. Moreover, a state-space description of any filter transfer function should be optimized for dynamic range, sensitivity, sparsity and the coefficient values [1], [4].

### B. Orthononormal Ladder Structure

Among known standard state-space descriptions, such as the canonical, the diagonal and the modal, the orthonormal ladder form is notable since it is by definition semi-optimized for dynamic range due to the specific structure of the matrices. Furthermore, since it is derived from a ladder structure, it is intrinsically less sensitive and the matrices are highly sparse. A detailed explanation of the procedure to derive the orthonormal ladder form can be found in [5].

With a state-space approach, the filter can be optimized for dynamic range, sensitivity, sparsity and coefficient values. A low sensitivity suppresses the effect of component variations on the transfer function. It can be proved that a filter that is optimized for dynamic range is also optimized for sensitivity [6]. The sparsity of the matrices directly determines the circuit complexity. State-space descriptions of filters with more zero elements require less hardware and are likely to consume lower power. Thus, it is therefore an important design aspect of state-space filters.

In respect to a fully optimized and fully dense state-space description, the resulting semi-optimal orthonormal filter structure differs only by about 2 dB in dynamic range. The *A, B, C,* and *D* matrices of the defined transfer function are as follows:

Matrix A:

| | | | | | | | |
|---|---|---|---|---|---|---|---|
| 0 | 2.122e9 | 0 | 0 | 0 | 0 | 0 | 0 |
| -2.122e9 | 0 | 6.859e8 | 0 | 0 | 0 | 0 | 0 |
| 0 | -6.859e8 | 0 | 3.933e9 | 0 | 0 | 0 | 0 |
| 0 | 0 | -3.933e9 | 0 | 10.81e9 | 0 | 0 | 0 |
| 0 | 0 | 0 | -10.81e9 | 0 | 10.69e9 | 0 | 0 |
| 0 | 0 | 0 | 0 | -10.69e9 | 0 | 7.77e9 | 0 |
| 0 | 0 | 0 | 0 | 0 | -7.77e9 | 0 | 1.47e10 |
| 0 | 0 | 0 | 0 | 0 | 0 | -1.47e10 | -1.62e10 |

Matrix B:

| | | | | | | | |
|---|---|---|---|---|---|---|---|
| 0 | 0 | 0 | 0 | 0 | 0 | 0 | 71732 |

Matrix C:

| | | | | | | | |
|---|---|---|---|---|---|---|---|
| 3.048e+4 | -1.64e-10 | -9.022e+4 | 2.476e-11 | 1.026e+5 | 4.307e-11 | 8.596e+4 | -2.253e+4 |

Matrix D:

| |
|---|
| 0.09998 |

### C. Scaling –Capacitance and Coefficient Values

Transconductance amplifiers will form the basic building blocks to implement the state-space description of the band-pass filter. The integrators are implemented as capacitors with a normalized value of 1 F. The corresponding matrices *A*, *B*, *C* and *D* have extremely large coefficients corresponding to large gm values, which are not physically feasible at circuit level. By scaling the capacitors (*cap*=1 pF), one consequently scales matrices *A* and *C*. Coefficients of matrices *B* and *D* can too be down scaled by $\alpha_1$ and $\alpha_2$ respectively, without affecting the response of the filter.

$$\begin{aligned} A^* &= cap \cdot A \\ B^* &= \alpha_1 B \\ C^* &= \alpha_2 \cdot cap \cdot C \\ D^* &= \alpha_1 \cdot \alpha_2 \end{aligned} \tag{1}$$

The block diagram of the state-space filter is shown in Fig. 3 and has 22 non-zero coefficients.

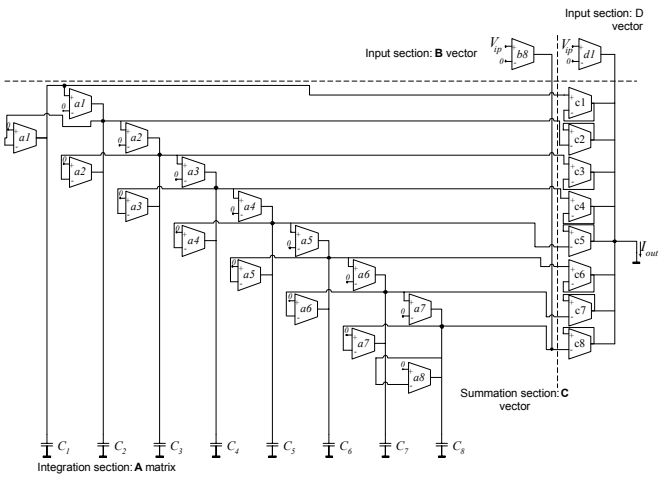


Fig. 3. Complete state-space filter structure

Once the block diagram has been recognized, a transconductance amplifier implements every coefficient.

## III. TRANSCONDUCTANCE AMPLIFIER

The transconductance amplifier is implemented using a negative feedback structure consisting of an active circuit, which implements a nullor and a feedback network (see Fig. 4). Theoretically, the nullor is an ideal block that has infinite transfer parameters.

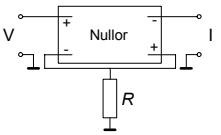


Fig. 4. Negative feedback amplifier with impedance in the feedback network

The orthonormal structure has both positive as well as negative coefficients. Since the structure in Fig. 4 can only implement a negative coefficient, a differential topology is used. Another advantage of using the latter is the cancellation of even order

distortion terms that arise from the actual nullor implementation, thus improving linearity.

The nullor (half circuit) is realized using a cascode (*CE-CG*) stage formed by transistors (*Q1-Q2*) at the input, and a non-inverting cross-coupled differential pair (*Q3-Q4*) at the output. The feedback network is made up of a resistor ***R*** (see Fig. 5).

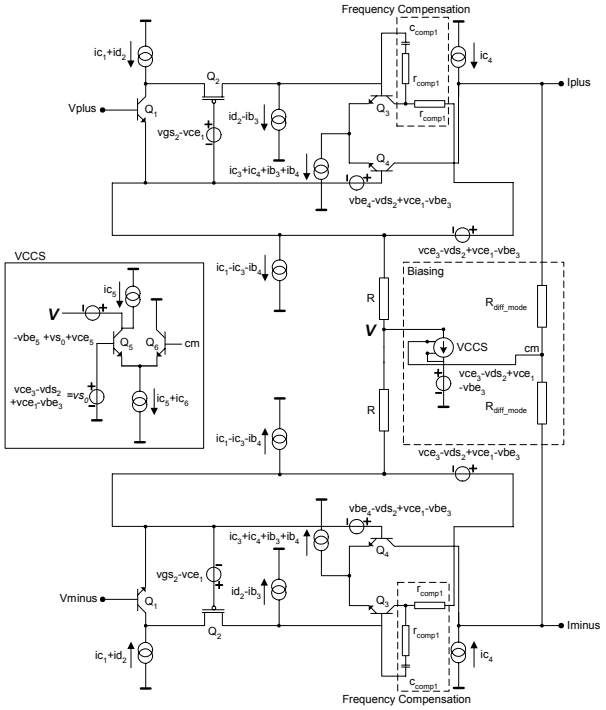


Fig. 5. 2-stage negative feedback gm amplifier

The CB-stage not only presents an output resistance that is larger by $g_{m2}r_{ds2}$ but also reduces Miller's effect of the CE-stage [7]. As compared to a single-stage implementation, a 2-stage nullor improves the loop gain, which yields higher linearity as well as bandwidth [7] at the expense of power consumption. In reference to stability, frequency compensation in the form of pole-zero cancellation is also applied to this transconductance amplifier. For biasing of the differential structure, the common-mode voltage is sensed at the outputs and is compared to the desired reference voltage using a voltage-controlled-current source (*VCCS*). Its implementation is shown at left in Fig. 5. The output current delivered by the VCCS is then applied to a virtual ground node, ***V***.

The small-signal behavior of the transconductance cell will now be analyzed.

### *A. Small-signal Analysis*

The integrating capacitors (*Cs*) at the input and output have also been taken into account.

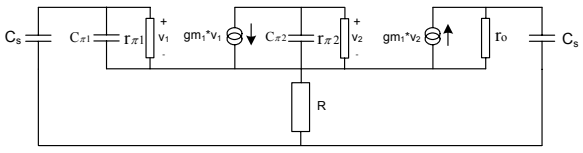


Fig. 6. Small signal model of the gm cell

For negative feedback amplifiers [7], the closed loop transfer (*At*) can be written in terms of the loop gain $A\beta(s)$ as,

$$At = -\xi \cdot \nu \cdot At_{\infty} \cdot \left[\frac{-A\beta(s)}{1-A\beta(s)}\right] \tag{2}$$

where $\nu$ and $\xi$ represent the input and output coupling factors and both are assumed to be equal to one.

$At_{\infty}$ is defined as,

$$At_{\infty} = -\frac{1}{\beta} \tag{3}$$

where $\beta$ is the feedback transfer. Now $A\beta(s)$ can be expressed as,

$$A\beta(s) = \left[-gm1\right]\cdot\left[\frac{r\pi_1}{1+s(r\pi_1 \cdot c\pi_1)}\right]\cdot\left[gm_2\right]\cdot\left[\frac{r\pi_2}{1+s(r\pi_2 \cdot c\pi_2)}\right]\cdot \left[\frac{R}{R+\left(\frac{1}{s\cdot cs}+\frac{r\pi_1}{1+s(r\pi_1\cdot c\pi_1)}\right)}\right]\cdot\left[\frac{r_o}{r_o+\frac{1}{s\cdot cs}+\left(R\,//\left(\frac{1}{s\cdot cs}+\frac{r\pi_1}{1+s(r\pi_1\cdot c\pi_1)}\right)\right)}\right] \tag{4}$$

where $gm_1$ and $gm_2$ are the transistor transconductances of the CE-stage and the differential pair, respectively, $r\pi_1, c\pi_1$ and $r\pi_2, c\pi_2$ are the base-emitter resistances and capacitances of $Q_1$ and $Q_{3\text{-}4}$, respectively and $R$ is the feedback resistance. Note that for simplicity, terms with *C*s (i.e. integrating capacitances of matrix *A*) will be neglected.

Simplifying by substituting (5) in (4) and assuming that $r_o$>>1,

$$\beta f_2 = \left[gm_2 \cdot r\pi_2\right];\ Z\pi_1 = \left[\frac{r\pi_1}{1+s(r\pi_1\cdot c\pi_1)}\right];\ Zs = \left[\frac{1}{s\cdot cs}\right] \tag{5}$$

one obtains,

$$A\beta(s) = \left[-gm_1\cdot \beta f_2\right]\cdot\left[\frac{R}{R+(Zs+Z\pi_1)}\right]\cdot Z\pi_1\cdot\left[\frac{1}{1+s(r\pi_2\cdot c\pi_2)}\right] \tag{6}$$

Substituting (6) in (2) and for large enough loop gains, the transfer is accurately determined by the feedback transfer $\beta$.

$$At = -\frac{1}{R}\cdot\left[\frac{-A\beta(s)}{1-A\beta(s)}\right] \approx -\frac{1}{R} \tag{7}$$

The DC-loop gain poles product ($LP_2$) predicts the bandwidth of the system and is stated in (7).

$$LP_2 \approx \left|A\beta(0)\right|\cdot\left|p_1\right|\cdot\left|p_2\right| \tag{8}$$

Substituting dc loop gain $A\beta(0)$ (9), closed loop poles $p_1$ and $p_2$ ((10) and (11), respectively) in (8),

$$A\beta(0) = \left[-gm_1\cdot\beta f_2\right]\cdot\left[\frac{R}{R+r\pi_1}\right]\cdot r\pi_1 \tag{9}$$

$$p_1 = \left[\frac{-1}{2\pi(r\pi_2\cdot c\pi_2)}\right] \tag{10}$$

$$p_2 = \left[\frac{-1}{2\pi(R\,//\,r\pi_1)\cdot c\pi_1}\right] \tag{11}$$

the bandwidth, *BW*, of the proposed 2-stage transconductance amplifier is approximately equal to the geometric mean of the transit frequencies of the respective stages [7].

$$LP_2 \approx f_{T1}\cdot f_{T2} \rightarrow BW \approx \sqrt{LP_2} \approx f_T \tag{12}$$

The influence on the transfer by the non-ideal coupling at the input and output modeled via ($\xi$) and ($\nu$) [7], respectively, needs to be taken into account. This aspect will result in a *BW* to some extent lower than $f_T$. The gm-C topology is implemented in IBM's 0.18 µm Bi-CMOS technology. In the same technology, the bias sources in

Fig. 5 are implemented using current mirrors with multiple outputs. All parasitic sources are also accounted for.

## IV. Simulation Results

Fig. 7 shows the magnitude and phase response of the stand-alone transconductance amplifier, which is used in the band-pass filter. Both the magnitude and the phase demonstrate a relatively flat response up to about 3 GHz.

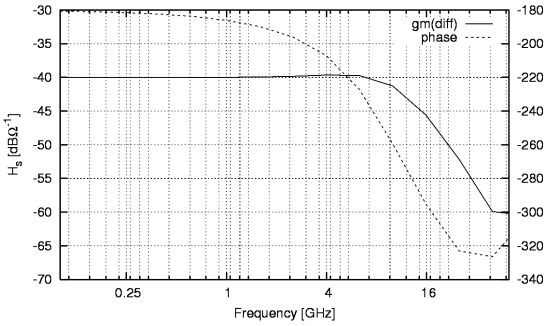


Fig. 7. Magnitude and phase transfer of stand-alone gm cell

From Fig. 8 it is clear that the high-frequency response of the entire filter is preserved at the cost of forfeiting some of the pass-band at lower frequencies. By scaling down the capacitance even lower than 1 pF as well as the coefficients in the matrices *A* and *C*, a superior transfer response is attainable because of the trade-off between bandwidth and gain.

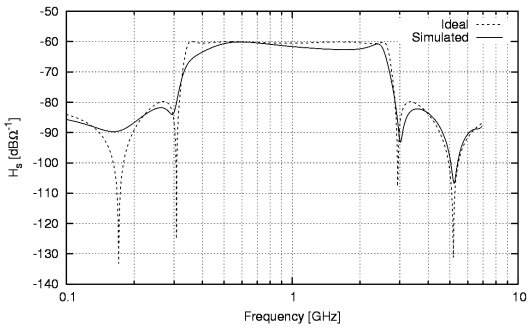


Fig. 8. Transfer of elliptic band-pass filter

Finally, by randomly varying (i.e. 25 iterations) the component tolerances as well as the model parameters between their specified tolerance limits, a Monte Carlo analysis is run in order to estimate the circuit's sensitivity. From Fig. 9 it is inferred that the transfer of the filter is relatively unlikely to show a substantial discrepancy as a result of process variations.

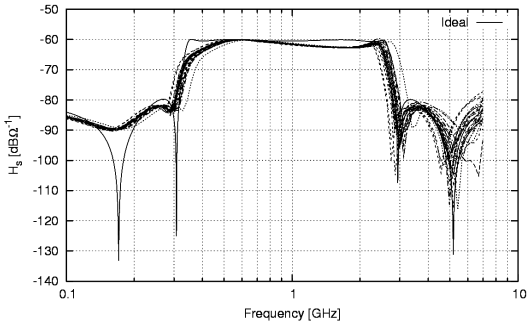


Fig. 9. Sensitivity analyses – Monte Carlo

Table I highlights the simulation parameters of the band-pass filter.

Table 1 Simulation Parameters

| Specifications | Simulated (@ 1GHz) |
|---|---|
| 1-dB compression pt. at | 565 mV |
| 3-dB compression pt. at | 575 mV |
| Dynamic range at 1-dB compression pt. (SNR) | +47.5 dB |
| IVIP3 (third-order input referred voltage intercept pt.) | +14 dBV |
| OIIP3 (third-order output referred current intercept pt.) | -47.6 dBA |
| Current consumption | 90 mA @ 1.8 V |
| Process | IBM Bi-CMOS 0.18µm |

## V. Conclusions

An interference rejection band-pass filter is to be used in the *QDAR* has been presented. An eighth order transfer function for an elliptic filter is selected. Subsequently, an orthonormal state-space approach is adopted, which fulfills the requirements of dynamic range, sensitivity, and sparsity. The coefficients are down scaled in conjunction with capacitance values. Each element of the filter is implemented at the circuit level using a novel negative feedback 2-stage gm amplifier. Simulation results in IBM's Bi-CMOS 0.18 µm technology (see Table 1) show that the interference rejection filter requires a total current 90 mA at a 1.8 V power supply. The 1-dB compression point of the filter is at 565 mV and the SNR is 47.5 dB.

## VI. References


[1] S.A.P. Haddad, S. Bagga and W.A. Serdijn, "Log-Domain Wavelet Bases," in *Proceedings IEEE International Symposium of Circuits and Systems*, May 2004

[2] R.T. Hoctor and H.W. Tomlinson, "Delay-Hopped Transmitted-Reference RF Communications," *Proceedings of the IEEE Conference on Ultra Wideband Systems and Technologies*, pp. 265-270, May 2002

[3] Simon Lee, S. Bagga and W.A. Serdijn, "A Quadrature Downconversion Autocorrelation Receiver Architecture for UWB," Joint *UWBST and IWUWBS*, May 2004

[4] D. Rocha, "Optimal Design of Analogue Low-Power Systems: A strongly directional hearing-aid adapter," PhD Thesis, Delft University of Technology, 2003

[5] D.A. Johns, W.M. Snelgrove and A.S. Sedra, "Orthonormal Ladder Filters," *IEEE Transactions on Circuits and Systems*, vol. 36, pp. 337-343, March 1989

[6] G. Groenewold,"*Optimal dynamic range integrators*", IEEE Transactions on Circuits and Systems, Volume: 39, Issue: 8, Aug. 1992, Pages: 614 - 627

[7] C.J.M.Verhoeven, A. van Staveren, G.L.E. Monna M.H.L. Kouwenhoven and E. Yildiz, "Structured Electronic Design: Negative-Feedback Amplifiers", *Kluwer Academic Publishers*, 2003